

NLTE ANALYSIS OF HIGH-RESOLUTION *H*-BAND SPECTRA. I. NEUTRAL SILICON\*JUNBO ZHANG<sup>1,2</sup>, JIANRONG SHI<sup>1,2</sup>, KAIKE PAN<sup>3</sup>, CARLOS ALLENDE PRIETO<sup>4,5</sup>, AND CHAO LIU<sup>1</sup><sup>1</sup>Key Laboratory of Optical Astronomy, National Astronomical Observatories, Chinese Academy of Sciences, A20 Datun Road, Chaoyang District, Beijing 100012, China<sup>2</sup>School of Astronomy and Space Science, University of Chinese Academy of Sciences, Beijing 100049, China; [sjr@bao.ac.cn](mailto:sjr@bao.ac.cn)<sup>3</sup>Apache Point Observatory and New Mexico State University, P.O. Box 59, Sunspot, NM, 88349-0059, USA<sup>4</sup>Instituto de Astrofísica de Canarias, E-38205 La Laguna, Tenerife, Spain<sup>5</sup>Departamento de Astrofísica, Universidad de La Laguna, E-38206 La Laguna, Tenerife, Spain

Received 2016 February 26; revised 2016 October 13; accepted 2016 October 14; published 2016 December 13

## ABSTRACT

We investigated the reliability of our silicon atomic model and the influence of non-local thermodynamical equilibrium (NLTE) on the formation of neutral silicon (Si I) lines in the near-infrared (near-IR) *H*-band. We derived the differential Si abundances for 13 sample stars with high-resolution *H*-band spectra from the Apache Point Observatory Galactic Evolution Experiment (APOGEE), as well as from optical spectra, both under local thermodynamical equilibrium (LTE) and NLTE conditions. We found that the differences between the Si abundances derived from the *H*-band and from optical lines for the same stars are less than 0.1 dex when the NLTE effects are included, and that NLTE reduces the line-to-line scatter in the *H*-band spectra for most sample stars. These results suggest that our Si atomic model is appropriate for studying the formation of *H*-band Si lines. Our calculations show that the NLTE corrections of the Si I *H*-band lines are negative, i.e., the final Si abundances will be overestimated in LTE. The corrections for strong lines depend on surface gravity, and tend to be larger for giants, reaching  $\sim -0.2$  dex in our sample, and up to  $\sim -0.4$  dex in extreme cases of APOGEE targets. Thus, the NLTE effects should be included in deriving silicon abundances from *H*-band Si I lines, especially for the cases where only strong lines are available.

*Key words:* line: formation – line: profiles – stars: abundances – stars: atmospheres

## 1. INTRODUCTION

Silicon is an important  $\alpha$ -element mainly produced during oxygen and neon burning, and is returned to the interstellar medium by Type II supernovae (SNe II; Woosley & Weaver 1995). SNe Ia may also produce a small fraction of silicon (Tsujiimoto et al. 1995). Silicon is an important element of the interstellar dust, one of the main electron contributors (only next to Fe and Mg) in the atmospheres of late-type stars (Holweger 1973; Wedemeyer 2001). The silicon abundance is often used as a tracer to explore the formation and evolution of the solar system (Johnson et al. 2011; Zambardi et al. 2013) and to study the Galactic structure, chemical enrichment history, and the origin of the Galaxy in many studies. For example, the silicon abundance, combined with other  $\alpha$ -elements, is often adopted as an indicator to distinguish stars from different populations, namely thick- and thin-disk populations (Lee et al. 2011). A series of studies, e.g., Bensby et al. (2005, 2014), Reddy et al. (2003, 2006), Nissen & Schuster (2010), and Zhang et al. (2011), have observed many high-resolution spectra and have derived accurate silicon abundances. Compared with different Galactic evolution models, e.g., Samland (1998), Goswami & Prantzos (2000), Romano et al. (2010) and Kobayashi et al. (2011), these abundances can help astronomers to understand the chemical enrichment history and the origin of the Galaxy. Thus, an accurate measurement of silicon abundances is necessary for many astrophysical applications.

Kamp (1973, 1978, 1982) calculated theoretical equivalent widths and profiles for silicon lines in both local thermodynamical equilibrium (LTE) and nonlocal thermodynamical equilibrium (NLTE) and compared them with observational data of a dozen early-type stars. The results indicate that the NLTE calculations provided better agreement with observations. The deviations from LTE on Si abundances in the photospheres of the Sun and Vega have been investigated by Wedemeyer (2001), who found that the mean NLTE correction for Si was  $\sim -0.01$  dex for the Sun, and  $\sim -0.054$  dex for Vega. This indicated that the NLTE effects on the Si abundance in the Sun could be neglected, which was confirmed by Shi et al. (2008). Later on, Shi et al. (2009, 2011) systematically investigated the NLTE effects on the derived silicon abundances in the atmospheres of metal-poor stars based on visible lines, and found that the NLTE effects are large for the two strong UV lines at 3905 and 4103 Å, especially for warm metal-poor stars. Shi et al. (2012) extended the study to the near-IR *J*-band Si lines, and found that the NLTE effects depend on surface gravities becoming higher for giants. Recently, Bergemann et al. (2013) investigated the NLTE effects on the *J*-band Si lines for red supergiants, and confirmed that Si abundance based on NLTE is significantly lower than that from LTE.

Until very recently, almost all observed high-resolution spectra are from UV, optical, and near-IR *J* bands, therefore previous studies on NLTE Si abundance are for spectral lines in these three bands. The situation has changed since the Apache Point Observatory Galactic Evolution Experiment (APOGEE) survey<sup>6</sup> (Majewski et al. 2015) (as part of SDSS-III, Eisenstein et al. 2011) started to take high-resolution IR *H*-band spectra

\* Based on observations collected with the 2.16 m telescope at Xinglong station, National Astronomical Observatories, Chinese Academy of Sciences, the 2.2 m telescope at the Calar Alto Observatory, the 1.88 m reflector at the Okayama Astrophysical Observatory, the Kitt Peak coude feed telescope, and the McMath-Pierce solar telescope and the coude focus of the Mayall 4 m reflector at Kitt Peak.

<sup>6</sup> <http://www.sdss.org/surveys/apogee>

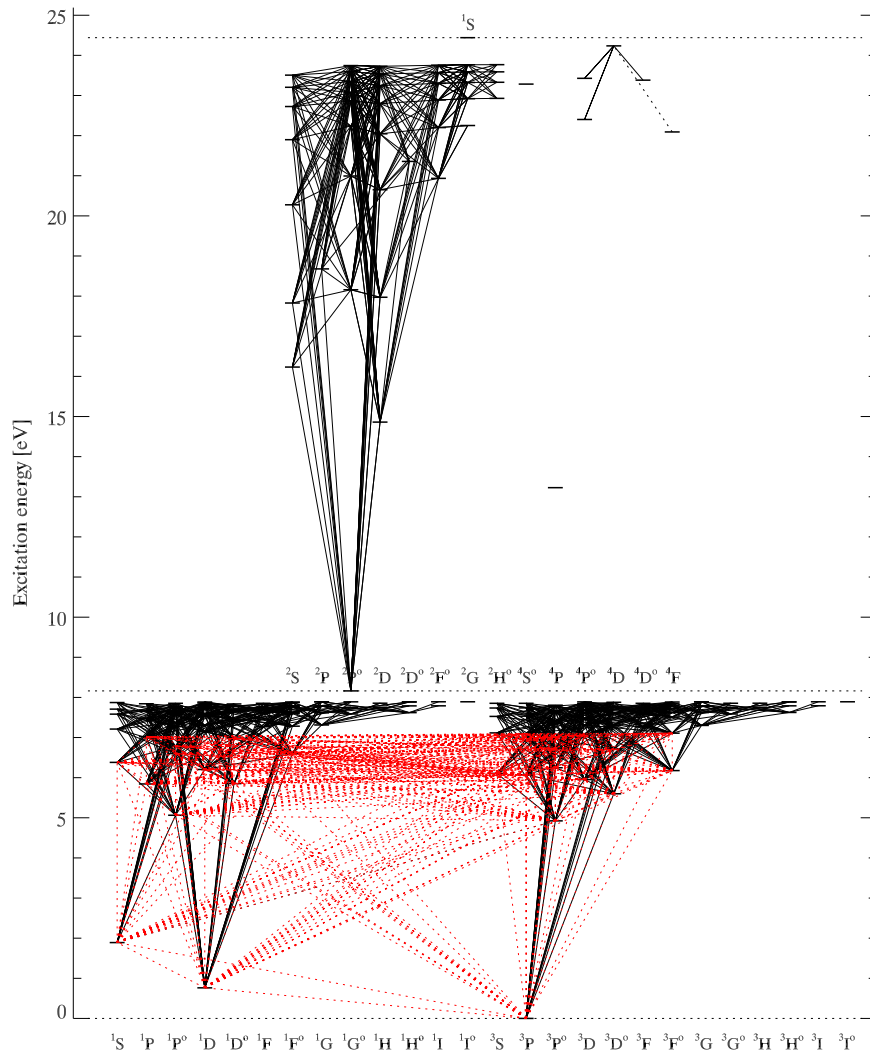


**Figure 1.** Grotrian diagram of the silicon model atom. Si II quartets are neglected. Allowed transitions are plotted as black continuous lines, the forbidden Si I 4103 Å line is a black dotted line. Transitions of Si I between 26 low-lying energy terms presented by Belyaev et al. (2014) are shown with red dotted lines.

for several hundred thousands stars. Thus, it is highly desirable to extend the NLTE investigations to the  $H$  band, where there are a dozen Si I lines that are clearly seen in APOGEE spectra.

Since 2011, the APOGEE survey employs a fiber spectrograph that simultaneously records 300 spectra in the  $H$  band between 1.51 and 1.70  $\mu\text{m}$  at a spectral resolution of  $R \sim 22,500$ . Detailed information about the instrument was provided by Wilson et al. (2010). Taking advantage of the reduced effect of extinction in the IR  $H$  band, APOGEE has observed  $\sim 150,000$  stars, predominantly red giants in all major Galactic components that are accessible from the Apache Point Observatory (APO) (Holtzman et al. 2015; Majewski et al. 2015). The spectra have been included in the SDSS Data Release 10 (DR10) (Ahn et al. 2014) and SDSS Data Release 12 (DR12) (Alam et al. 2015). The data provide a promising way to trace and explore the formation history of the Galaxy, and they are revolutionizing our knowledge on the kinematical and chemical enrichment history of all Galactic stellar populations.

The APOGEE Stellar Parameters and Chemical Abundances Pipeline (ASPCAP) provides the physical and chemical

parameters for the APOGEE stars (García Pérez et al. 2016). In addition to the stellar parameters, i.e., the effective temperature ( $T_{\text{eff}}$ ), surface gravity ( $\log g$ ), and metallicity ( $[M/H]$ ), ASPCAP delivers individual chemical abundances for 15 elements. The accuracy of these derived stellar fundamental parameters and chemical compositions may be compromised. NLTE effects are enhanced by the characteristic low densities found in the atmospheres of giants and the absolute reduction in collision rates, which affects the atomic populations (Mészáros et al. 2013). Hawkins et al. (2016) have performed an independent procedure to determine the chemical abundances of the APOGEE + *Kepler* stellar sample (APO-KASC), and they inferred that the discrepant phenomenon for some elements is likely due to the NLTE effects. As part of a series of studies on the NLTE analysis of  $H$ -band lines for several important elements, e.g., Na, Mg, Al, Si, K, Ca, and Fe, this work aims to validate the Si atomic model and to investigate how the abundances derived from the Si  $H$ -band transitions are affected by departures from LTE.

This paper is organized as follows. In Section 2 we briefly introduce our adopted Si model atom and NLTE calculation

**Table 1**  
Characteristics of the Observed Optical Spectra

Star	$V_{\text{mag}}^{\text{a}}$ (mag)	Telescope/Spectrograph	Observing Run, Observer	Spectral Range ( $\text{\AA}$ )	$R$	S/N
Arcturus	-0.05	KPCFT/ES	1998-99, K. Hinkle et al.	3727-9300	150,000	$\sim 1000$
HD 87	5.55	1.88 m/HIDES	2007 Jul, Anonymous <sup>b</sup>	5000-6200	67,000	$\geq 150$
HD 6582	5.17	2.2 m/FOCES	1995 Sep, K. Fuhrmann	4000-7000	35,000	$\geq 150$
HD 6920	5.67	2.2 m/FOCES	1997 Feb, K. Fuhrmann	4000-9000	60,000	$\sim 200$
HD 22675	5.86	1.88 m/HIDES	2010 Jan, B. Sato	4000-7540	67,000	$\sim 300$
HD 31501	8.15	2.16 m/CES	2008 Jan, J. R. Shi	5600-8800	40,000	$\geq 150$
HD 58367	4.99	1.88 m/HIDES	2004 Feb, Anonymous <sup>b</sup>	5000-6200	67,000	$\geq 150$
HD 67447	5.34	2.16 m/FOES	2015 Jan, J. B. Zhang	3900-7260	50,000	$\geq 150$
HD 102870	3.59	2.2 m/FOCES	1997 May, K. Fuhrmann	4000-9000	60,000	$\sim 200$
HD 103095	6.42	2.2 m/FOCES	2000 May, K. Fuhrmann	4000-9000	60,000	$\sim 200$
HD 121370	2.68	2.2 m/FOCES	1998 Dec, K. Fuhrmann	4000-9000	60,000	$\sim 200$
HD 148816	7.27	2.2 m/FOCES	2001 Aug, T. Gehren	4000-9000	60,000	$\sim 200$
HD 177249	5.51	1.88 m/HIDES	2004 Nov, Anonymous <sup>b</sup>	5000-6200	67,000	$\sim 300$

#### Notes.

<sup>a</sup> Visual magnitudes are derived from the *Hipparcos* Main Catalogue (ESA 1997) through VizieR (<http://vizier.u-strasbg.fr/viz-bin/VizieR>).

<sup>b</sup> Spectra were provided by Y. Takeda, B. Sato, and Y. J. Liu et al. The observer written in the spectra header is anonymous, and it is difficult for us to identify the actual observers.

codes, while the selection of the sample stars and the observed spectra are described in Section 3. The stellar parameters of our sample stars are determined in Section 4, and the Si abundances derived from both the  $H$ -band and optical lines for the sample stars under LTE and NLTE analyses are presented in Section 5. Finally, the conclusions are given in Section 6.

## 2. METHOD OF NLTE CALCULATIONS

### 2.1. Model Atom of Silicon

The Si atomic model that we used here is similar to that of Shi et al. (2008), which includes the most important 132 terms of Si I, 41 terms of Si II, and the Si III ground state. The radiative data are taken from Nahar & Pradhan (1993). Lacking accurate values for inelastic collisions with neutral hydrogen, Shi et al. (2008) suggested  $S_{\text{H}} = 0.1$  by fitting solar strong infrared Si I lines. Fortunately, Belyaev et al. (2014) calculated the cross sections and rate coefficients for inelastic processes in  $\text{Si} + \text{H}$  and  $\text{Si}^+ + \text{H}^-$  collisions for all transitions between 26 low-lying states plus the ionic state. We revised the Si atomic model by including all cross sections from Belyaev et al. (2014) whenever available; otherwise,  $S_{\text{H}} = 0.1$  was adopted. The Grotrian diagram of the silicon model atom with the transitions between 26 low-lying energy terms relative to Belyaev et al. (2014) is shown in Figure 1. In this work, we also calculated the NLTE line profiles for the Sun and Arcturus with four different collision treatments, i.e., the Drawin recipe with  $S_{\text{H}} = 0.0, 0.1,$  and  $1.0,$  and the treatment from Belyaev et al. (2014). The results are depicted in Figures 3 and 4, respectively. Our adopted stellar parameters for the Sun are  $T_{\text{eff}} = 5777 \text{ K},$   $[\text{Fe}/\text{H}] = 0.0 \text{ dex},$   $\log g = 4.44 \text{ dex},$  and  $\xi_t = 0.9 \text{ km s}^{-1}.$  As shown in these two groups of figures, the calculated NLTE line profiles with  $S_{\text{H}} = 0.1$  and the treatment from Belyaev et al. (2014) can fit the observed spectral lines well for both the Sun and Arcturus; for the strong lines at 15888 and 16680  $\text{\AA},$  the synthetic line profiles with  $S_{\text{H}} = 1.0$  are shallower than the observed lines, while those with  $S_{\text{H}} = 0.0$  are slightly deeper, with the same silicon abundance.

### 2.2. Model Atmospheres

We adopted MARCS atmospheric models,<sup>7</sup> described in detail by Gustafsson et al. (2008). The MARCS models come in two types, the plane-parallel and the spherically symmetric model atmospheres. The models with low surface gravities ( $-1.0 \leq \log g \leq 3.5$ ) are calculated in spherical geometry, while the plane-parallel models are adopted for stars with  $3.0 \leq \log g \leq 5.5.$  Gustafsson et al. (2008) suggested that sphericity effects are generally important for the temperature structures of low-gravity stars. In this paper, spherical model atmospheres are used for stars with  $\log g \leq 3.5,$  and plane-parallel model atmospheres for the other stars. They are interpolated with a FORTRAN-based routine coded by Thomas Masseron.<sup>8</sup>

The main characteristics of the MARCS model atmospheres are summarized below (Gustafsson et al. 2008).

1. The basic chemical composition of the Sun in model atmospheres is that listed by Grevesse et al. (2007). The adopted solar Si abundance is 7.51 dex, which is the Si abundance based on a three-dimensional (3D) LTE and also the meteoritic Si abundance. Amarsi & Asplund (2016) recently based on 3D NLTE calculations and also found the same solar Si abundance.
2. The  $\alpha$ -enhancement is included.

$$[\alpha/\text{Fe}] = \begin{cases} 0.4 \cdot |[\text{Fe}/\text{H}]| & \text{if } -1.0 < [\text{Fe}/\text{H}] < 0.0 \\ 0.4 & \text{if } [\text{Fe}/\text{H}] \leq -1.0 \end{cases}.$$

3. The adopted mixing-length parameter  $l/H_{\text{p}}$  is 1.5 (Henyey et al. 1965).

### 2.3. Statistical Equilibrium Codes

A revised DETAIL program of Butler & Giddings (1985) was adopted to solve the coupled statistical equilibrium and the radiative transfer equations. This program is based on an

<sup>7</sup> <http://marcs.astro.uu.se>

<sup>8</sup> <http://marcs.astro.uu.se/software.php>

**Table 2**  
Comparison of Stellar Parameters with Other Studies

Star	$T_{\text{eff}}$ (K)	$\log g$ (cgs)	[Fe/H]	$\xi_r$ ( $\text{km s}^{-1}$ )	Reference <sup>a</sup>
Arcturus	4275	1.67	-0.58	1.60	This study
	4286	1.66	-0.52	1.74	RAM11
	4286	1.66	-0.48	1.74	SHE15
HD 87	5053	2.71	-0.10	1.35	This study
	5072	2.63	-0.10	1.35	TAK08
HD 6582	5390	4.42	-0.81	0.90	This study
	5387	4.45	-0.83	0.89	FUH98
HD 6920	5845	3.45	-0.06	1.40	This study
	5838	3.48	-0.05	1.35	FUH98
<u>HD 22675</u>	4901	2.76	-0.05	1.30	This study
	4878	2.50 <sup>b</sup>	-0.06	1.29	TAK08
		2.66 <sup>c</sup>	...	...	...
HD 31501	5320	4.45	-0.40	1.00	This study
	5326	4.41	-0.38	1.00	WAN09
HD 58367	4932	1.79	-0.18	2.00	This study
	4911	1.76	-0.14	2.04	TAK08
HD 67447	4933	2.17	-0.05	2.12	This study
	4974	2.12	-0.06	2.12	TAK08
HD 102870	6070	4.08	0.20	1.20	This study
	6085	4.04	0.14	1.38	FUH98
	6060	4.11	0.18	1.20	MAS11
HD 103095	5085	4.65	-1.35	0.80	This study
	5110	4.66	-1.35	0.85	FUH98
	5070	4.69	-1.35	0.80	MAS07
HD 121370	6020	3.80	0.28	1.40	This study
	6023	3.76	0.28	1.40	FUH98
HD 148816	5830	4.10	-0.73	1.40	This study
	5823	4.13	-0.73	1.40	NIS10
<u>HD 177249</u>	5273	2.66	0.03	1.65	This study
	5251	2.55 <sup>b</sup>	0.00	1.65	TAK08
	...	2.62 <sup>c</sup>	...	...	TAK08

**Notes.** Underlines mean that the stars are discussed in detail in Section 4.

<sup>a</sup> RAM11: Ramírez & Allende Prieto (2011), SHE15: Sheminova (2015), TAK08: Takeda et al. (2008), FUH98: Fuhrmann (1998), WAN09: Wang et al. (2009), MAS11: Mashonkina et al. (2011), MAS07: Mashonkina et al. (2007), NIS10: Nissen & Schuster (2010).

<sup>b</sup>  $\log g$ , derived from the spectroscopic method.

<sup>c</sup>  $\log g$ , derived from the parallax and evolution-track method.

accelerated lambda iteration scheme, following the approach described by Rybicki & Hummer (1991, 1992). In this paper, departure coefficients were computed with DETAIL and then fed to the spectrum synthesis software package Spectrum Investigation Utility (SIU), developed by Reetz (1991), to derive chemical abundances.

### 3. THE SAMPLE STARS AND THEIR SPECTRA

#### 3.1. Sample Selection

Although Shi et al. (2012) have demonstrated that their Si atomic model could provide consistent silicon abundances for the optical and infrared  $J$ -band spectra, we would like to check whether the atomic model can also be applied to the  $H$ -band Si I lines. We selected 13 FGK dwarfs and giants as sample stars for this test according to the following criteria: 1) they must have available high-resolution ( $R > 20,000$ ) and high signal-to-noise ratio ( $S/N > 100$ ) spectra both in the optical and  $H$  bands and 2) the selected stars should be representative of the typical stellar parameter range of the FGK stars ( $T_{\text{eff}} \sim 4000\text{--}6500$  K,

$\log g \sim 0.0\text{--}5.0$ , and  $[M/H] \sim -2.0\text{--}0.5$  dex). The final stellar parameters of sample stars span from 4275 to 6070 K for  $T_{\text{eff}}$ , from 1.67 to 4.65 for  $\log g$ , and from  $-1.35$  to 0.28 dex for  $[Fe/H]$ . However, there are no very metal-poor stars ( $[Fe/H] < -1.5$  dex) in our sample because the Si lines in the APOGEE spectra are weak for such stars. The IR and optical data are described in the following subsections.

#### 3.2. Infrared $H$ -band Spectra

The IR  $H$ -band spectra of our 13 sample stars are from the New Mexico State University (NMSU) 1m+APOGEE observations, and they are included in SDSS DR12. The 1m+APOGEE configuration is designed to observe nearby bright stars and to provide an improved calibration for the main APOGEE survey (Holtzman et al. 2015). A bundle of ten fibers was installed connecting the APOGEE instrument to the NMSU 1 m telescope. This configuration provides one science fiber and nine sky fibers per observation. Bright stars with a magnitude of  $0 < H < 8$  are observed in this configuration in dark time when the APOGEE instrument is not connected with the Sloan 2.5 m telescope. The spectra taken with the NMSU 1m+APOGEE are reduced and analyzed with the same software employed by the main survey (Nidever et al. 2015). We refer the reader to Feuillet et al. (2016) for more details. Since all 13 selected stars are bright, the S/N of APOGEE spectra of these stars are very high (e.g.,  $S/N \geq 400$  for Arcturus). As mentioned earlier, the resolution is about 22,500.

The high-resolution ( $R \sim 500,000$ ) solar infrared spectrum from the Kurucz website<sup>9</sup> was adopted in this study. It was obtained by James Brault at Kitt Peak and reduced by Robert L. Kurucz. We also employed the spectrum of Arcturus from the NOAO science archives,<sup>10</sup> which was recorded with the Fourier transform spectrometer (FTS, Hall et al. 1979) operated at the coude focus of the Mayall 4 m reflector at Kitt Peak. The detailed description of the observation was presented by Hinkle et al. (1995). The high-resolution ( $\sim 100,000$ ) and high S/N spectrum of Arcturus facilitates identifying the continuum, and is most efficient in recognizing blending lines.

#### 3.3. Optical Spectra

We adopted the optical solar spectrum of Kurucz et al. (1984). Six of our sample stars (HD 6582, HD 6920, HD 102870, HD 103095, HD 121370, and HD 148816) were observed with the fiber-coupled Cassegrain échelle spectrograph (FOCES; Pfeiffer et al. 1998) on the 2.2 m telescope at the Calar Alto Observatory. Spectra of HD 87, HD 22675, HD 58367, and HD 177249 were taken with the High Dispersion Échelle Spectrograph (HIDES) on the coude focus of the 1.88 m reflector at the Okayama Astrophysical Observatory (Izumiura 2003). The optical spectrum of Arcturus was obtained with the échelle spectrograph (ES) on the Kitt Peak coude feed telescope (KPCFT), with a typical resolving power of 150,000 and a S/N of about 1000 (Hinkle et al. 2000, 2005). Both HD 31501 and HD 67447 were observed using the 2.16 m telescope at Xinglong station, but with different spectrographs: for HD 31501 it was the Coude Échelle Spectrograph (CES; Zhao & Li 2001), and for HD 67447 with the fiber optics échelle spectrograph (FOES). The detailed

<sup>9</sup> <http://kurucz.harvard.edu/sun/irradiance2008/>

<sup>10</sup> <http://ast.noao.edu/data/other>

**Table 3**Atomic Data of the Silicon Optical and  $H$ -band Lines, the Derived LTE and NLTE Solar Silicon Abundance Based on  $\log gf$  from References and the NLTE Corrections for the Solar Silicon Lines

$\lambda$ (Å)	Transition	$\chi$ (eV)	$\log C_6$	$\log gf$	Reference	$\log \epsilon_{\odot}\text{Si}$ LTE (dex)	$\log \epsilon_{\odot}\text{Si}$ NLTE (dex)	$\log gf'$ LTE	$\log gf'$ NLTE	$\Delta_{\odot}$ (dex)
5701.104	$4s\ ^3P_1^o-5p\ ^3P_0$	4.930	-30.094	-2.05	GAR73, KEL08	7.60	7.60	-1.96	-1.96	0.00
5772.146	$4s\ ^1P_1^o-5p\ ^1S_0$	5.082	-30.087	-1.75	GAR73, KEL08	7.64	7.63	-1.62	-1.63	-0.01
6142.483	$3p^3\ ^3D_1^o-5f\ ^3D_3$	5.619	-29.669	-1.30	KUR07	7.37	7.37	-1.44	-1.44	0.00
6145.016	$3p^3\ ^3D_2^o-5f\ ^3G_3$	5.616	-29.669	-1.31	KUR07	7.45	7.45	-1.37	-1.37	0.00
6155.134	$3p^3\ ^3D_3^o-5f\ ^3G_4$	5.619	-29.669	-0.76	KUR07	7.50	7.49	-0.77	-0.78	-0.01
6237.319	$3p^3\ ^3D_1^o-5f\ ^3F_2$	5.614	-29.669	-0.98	KUR07	7.43	7.43	-1.06	-1.06	0.00
6243.815	$3p^3\ ^3D_2^o-5f\ ^3F_3$	5.616	-29.669	-1.24	KUR07	7.49	7.49	-1.26	-1.26	0.00
6244.466	$3p^3\ ^3D_2^o-5f\ ^1D_2$	5.616	-29.669	-1.09	KUR07	7.35	7.35	-1.25	-1.25	0.00
mean	...	...	...	...	...	7.48	7.48	...	...	...
$\sigma$	...	...	...	...	...	0.10	0.10	...	...	...
15888.440	$4s\ ^1P_1^o-4p\ ^1P_1$	5.082	-30.638	0.06	KUR07	7.58	7.57	0.13	0.12	-0.01
16380.177	$4p\ ^1P_1-3d\ ^1P_1^o$	5.863	-30.495	-0.47	KUR07	7.03	7.03	-0.95	-0.95	0.00
16680.810	$4p\ ^3D_3-3d\ ^3D_3^o$	5.984	-30.357	-0.14	KUR07	7.48	7.45	-0.17	-0.20	-0.03
16828.158	$4p\ ^3D_3-3d\ ^3D_2^o$	5.984	-30.357	-1.03	KUR07	7.41	7.41	-1.13	-1.13	0.00
mean	...	...	...	...	...	7.37	7.36	...	...	...
$\sigma$	...	...	...	...	...	0.24	0.24	...	...	...

**Note.** References to the  $\log gf$  values are GAR73: Garz (1973), KEL08: Kelleher & Podobedova (2008) and KUR07: Kurucz (2007). The  $\log C_6$  values were calculated according to Anstee & O'Mara (1991, 1995) and Barklem et al. (2000).  $\sigma$  refers to the statistical error. The  $\log gf'$  denotes that the  $gf$ -values were derived from the solar fits.

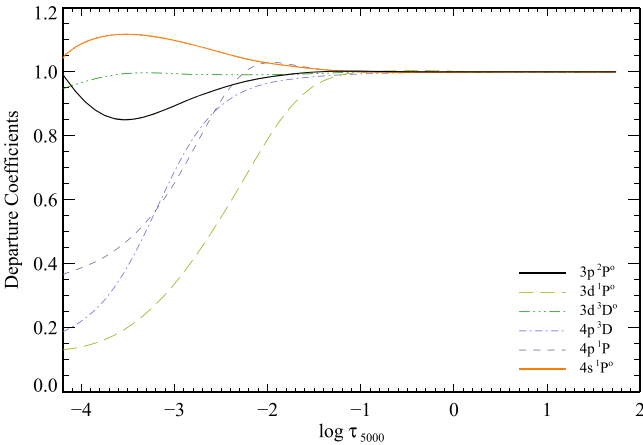


**Figure 2.** Departure coefficients  $b_i = N_i^{\text{NLTE}}/N_i^{\text{LTE}}$  as a function of the standard optical depth for HD 87.

observational information for the sample stars is listed in Table 1 (except for the Sun). It is worthwhile noting that all optical spectra have a resolving power better than 35,000 and a  $S/N \geq 150$ .

#### 4. STELLAR PARAMETERS

The stellar parameters of all 13 stars were determined via the spectroscopic approach. Specifically, the effective temperature and surface gravity were determined by fulfilling the excitation equilibrium of Fe I and the ionization equilibrium of Fe I and Fe II, respectively; the microturbulence velocity was determined by forcing  $[\text{Fe}/\text{H}]$  from different Fe I lines to be

independent of their equivalent widths. Table 8 gives the equivalent widths for our sample stars.

This process of determining stellar parameters is an iterative procedure. A set of initial parameters is needed to begin with. The initial temperature was derived from the Balmer lines ( $H_\alpha$  and  $H_\beta$ ) (Fuhrmann 1998) when these lines were available. Otherwise, it was obtained based on the color index ( $b - y$  or  $V - K$ ) employing the calibration given by Alonso et al. (1996, 1999, 2001). The initial surface gravity was estimated using the parallax method. There are 30 Fe I and 6 Fe II optical lines included in our analysis. The line data as well as the equivalent widths for the solar iron lines are listed in Table 6. Departures from LTE have been considered when determining the iron abundance based on the iron model atom from Mashonkina et al. (2011), and for the Sun and our sample stars, they are small, lower than 0.05 dex. In Table 6 we also present the solar LTE and NLTE iron abundances based on the oscillator strength ( $\log gf$ ) values recommended by the VALD3 database.<sup>11</sup> According to this table, the iron abundances derived from Fe I lines are  $7.56 \pm 0.13$  dex in LTE and  $7.60 \pm 0.13$  dex in NLTE, while they are  $7.49 \pm 0.04$  dex from Fe II lines in both cases. The statistical error for the Sun is uncomfortably large, up to 0.13 dex, thus we derived the empirical  $\log gf$  by fitting the solar spectrum and present the  $\log gf$  values derived from the NLTE solar fits in this table. The values of  $\log C_6$  were calculated referring to Anstee & O'Mara (1991, 1995) and Barklem et al. (2000). Based on multiple iterative processes, we estimate that the typical uncertainties of  $T_{\text{eff}}$ ,  $\log g$ ,  $[\text{Fe}/\text{H}]$ , and  $\xi_t$  are  $\pm 80$  K,  $\pm 0.1$  dex,  $\pm 0.08$  dex, and  $0.2 \text{ km s}^{-1}$ , respectively.

<sup>11</sup> <http://vald.astro.uu.se>

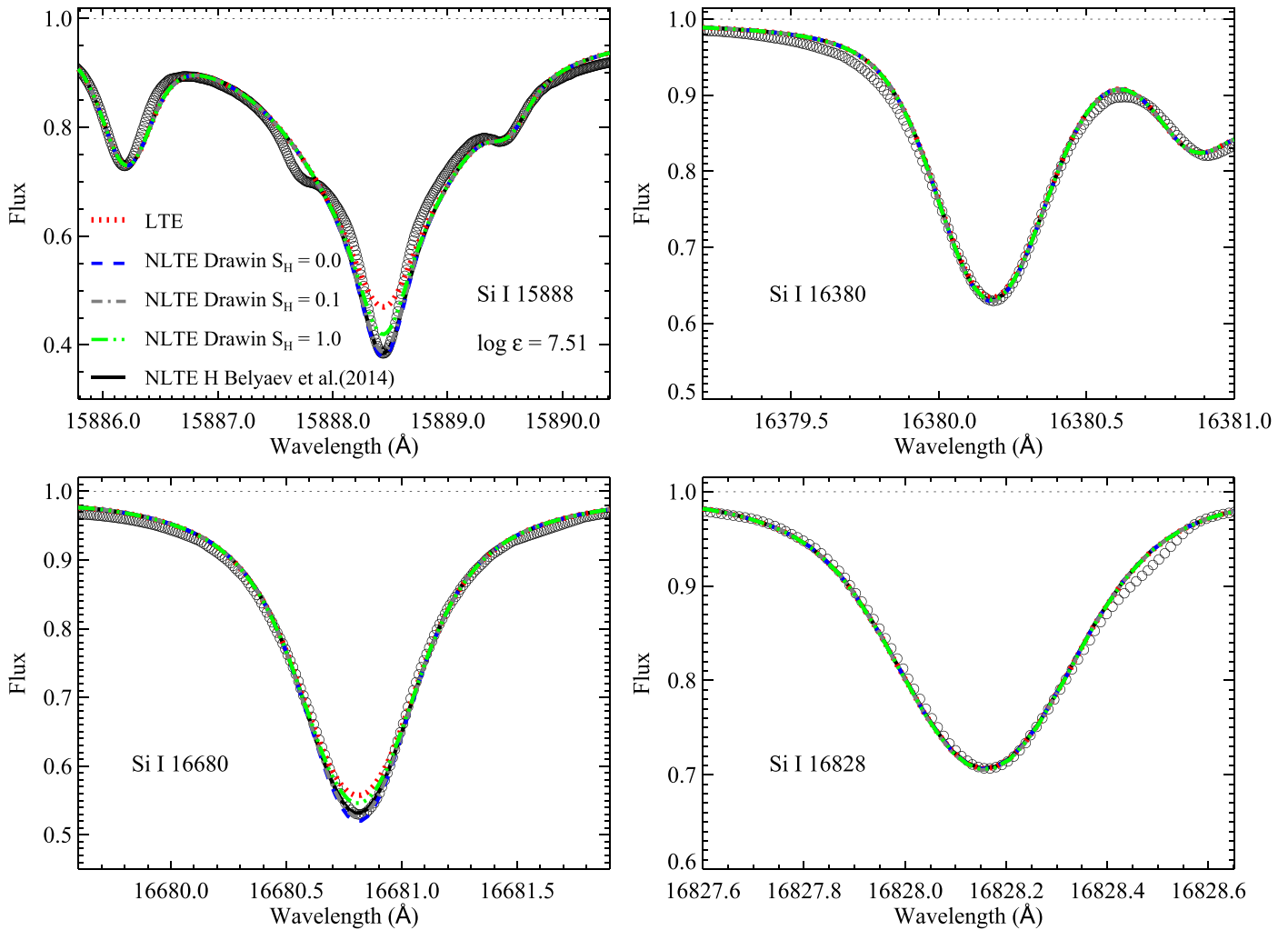


**Figure 3.** *H*-band solar Si I line profiles. The NLTE profiles with rates of collisions with hydrogen from Belyaev et al. (2014) and the Drawin recipe with  $S_H = 0.0$ , 0.1, 1.0, and LTE profiles compared with the observed spectrum (open circles), where the NLTE profiles with the Belyaev et al. (2014) treatment refer to the best fits.

The final derived stellar parameters, along with stellar parameters for the same stars from the literature, are presented in Table 2. Our derived values are consistent with those from literature, except  $\log g$  for HD 22675 and HD 177249. Our newly derived  $\log g$  values for the two stars are 0.26 and 0.11, respectively, higher than those determined by Takeda et al. (2008). We note that our spectroscopic  $\log g$  values agree well with those from the parallax method derived by Takeda et al. (2008). This may indicate that our spectroscopic surface gravities for these two stars are more accurate than those from Takeda et al. (2008).

## 5. NLTE CALCULATIONS FOR SAMPLE STARS

### 5.1. Line Data

#### 5.1.1. Infrared Atomic Line Data in the *H* band

Initially, we found 11 Si I lines in the *H*-band APOGEE spectra. A further investigation reveals that seven of them are very weak or heavily blended. As a result, only four lines were employed in this study. The details about them are presented in Table 3. The transitions are taken from the NIST database.<sup>12</sup>

<sup>12</sup> <http://physics.nist.gov/>

The van der Waals damping constants ( $\log C_6$ ) are extracted from Meléndez & Barbuy (1999), who calculated  $C_6$  based on the quantum-mechanical approximate cross sections provided by Anstee & O’Mara (1995); Barklem & O’Mara (1997) and Barklem et al. (1998). We derived the solar LTE and NLTE Si abundances using the  $gf$ -values referring to the references and found that the statistic errors are very large in both LTE and NLTE. In order to reduced the importance of oscillator strengths, therefore, we performed a line-to-line differential analysis and the  $gf$ -values derived from the LTE and NLTE solar spectrum fits are also listed in Table 3.

#### 5.1.2. Optical Atomic Line Data

We started with the same set of neutral Si optical lines used by Shi et al. (2009). An examination shows that the line at 3905 Å is severely blended with a CH line, and the line at 4103 Å falls in the wing of  $H_\delta$ , while the line at 5690 Å is blended with an iron line. These three transitions were excluded from our Si abundance analysis. The adopted eight Si I lines and line data are listed in Table 3. We also derived the solar Si abundance based on optical lines using the  $\log gf$  values from references. Although the mean Si abundance is consistent with the previous studies, the statistic error is also

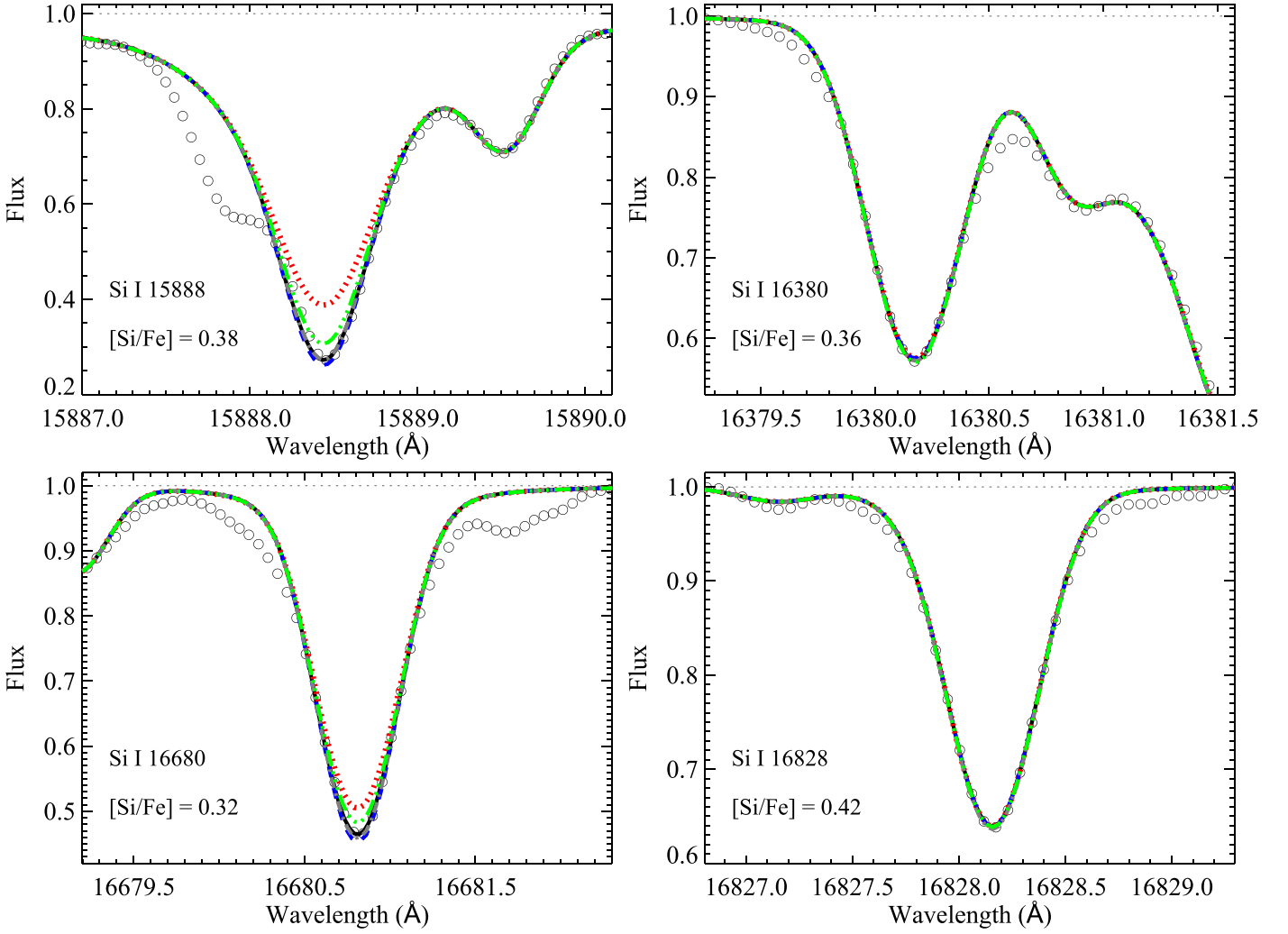


**Figure 4.** Similar to Figure 3, the NLTE and LTE profiles for Arcturus. Here the observed spectrum is from Hinkle et al. (1995).

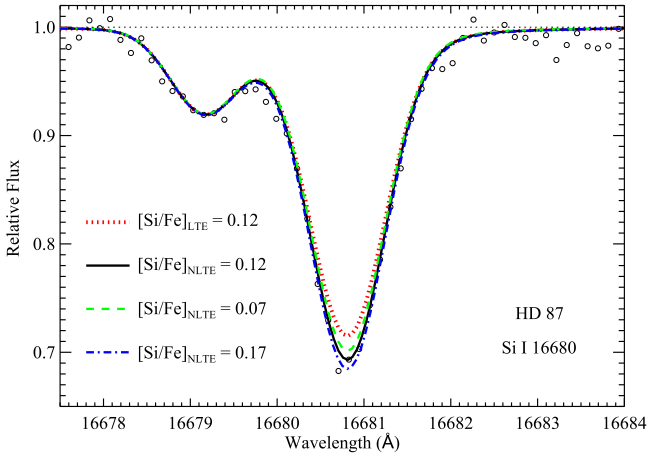


**Figure 5.** Spectrum synthesis of the Si I 16680 Å line for HD 87. The open circles are the observed spectrum. The black solid line is the best-fitting NLTE line profile, and the red dotted curve is the LTE profile with the same Si abundance. The other two lines are the synthetic spectra in NLTE with different [Si/Fe] (see the legend for details).

not satisfying, up to 0.1 dex. To be consistent with the situation for infrared lines, we also present the  $gf$ -values determined from the solar spectrum fitting. The  $C_6$  values were calculated

according to Anstee & O'Mara (1991, 1995) and Barklem et al. (2000).

## 5.2. NLTE Effects

### 5.2.1. Departures from LTE for the Si I H-band Lines

In Figure 2 we present the departure coefficients ( $b_i$ ) for the relevant Si I levels for  $H$ -band transitions and Si II ground state as a function of the optical depth at  $\lambda = 5000$  Å ( $\tau_{5000}$ ) for the model atmosphere of HD 87. Here, the departure coefficients ( $b_i$ ) are defined as  $b_i = n_i^{\text{NLTE}}/n_i^{\text{LTE}}$ , where  $n_i^{\text{NLTE}}$  and  $n_i^{\text{LTE}}$  represent the statistical equilibrium (NLTE) and thermal (LTE) atomic level number densities, respectively. It is found that the departure coefficients for the level  $3d^3D^0$  of Si I are near their thermal value ( $b_i \sim 1$ ) and the level  $4s^1P^0$  is overpopulated, while the other excitation levels,  $4p^1P$ ,  $4p^3D$ , and  $3d^1P^0$  are underpopulated as a result of photon loss (see Figure 2 for details).

As the first test of our atomic model, we have analyzed optical lines for the Sun. We confirmed that the NLTE corrections for optical silicon lines are negligible (Shi et al. 2008; Wedemeyer 2001; Bergemann et al. 2013). For the investigated four  $H$ -band Si lines, we found that the derived NLTE effects are also minor, and the largest effect is 0.03 dex

**Table 4**  
Stellar [Si/Fe] for the Individual Si I *H*-band Lines under LTE and NLTE Analyses

Star	15888 (Å)		16380 (Å)		16680 (Å)		16828 (Å)		$\sigma_{\text{line}}$	
	LTE	NLTE	LTE	NLTE	LTE	NLTE	LTE	NLTE	LTE	NLTE
Arcturus <sup>a</sup>	0.49	0.38	0.37	0.36	0.43	0.32	0.43	0.42	0.06	0.05
Arcturus <sup>b</sup>	0.50	0.38	0.34	0.33	0.44	0.34	0.44	0.43	0.08	0.06
HD 87	0.19	0.08	0.15	0.14	0.23	0.12	0.15	0.15	0.05	0.04
HD 6582	0.22	0.19	0.26	0.25	0.26	0.25	...	...	0.03	0.04
HD 6920	0.11	-0.01	-0.04	-0.05	0.10	-0.01	...	...	0.10	0.03
HD 22675	0.12	0.02	0.07	0.06	0.15	0.06	...	...	0.05	0.03
HD 31501	0.13	0.09	0.16	0.15	0.21	0.19	...	...	0.05	0.07
HD 58367	0.26	0.03	0.04	0.04	0.31	0.13	0.12	0.13	0.16	0.07
HD 67447	0.25	0.08	0.05	0.04	0.22	0.07	0.10	0.10	0.12	0.03
HD 102870	-0.02	-0.09	-0.07	-0.08	-0.04	-0.09	-0.08	-0.08	0.04	0.01
HD 103095	0.26	0.24	0.36	0.36	0.35	0.35	...	...	0.07	0.08
HD 121370	0.11	0.02	0.15	0.14	0.22	0.14	0.14	0.14	0.06	0.06
HD 148816	0.30	0.24	0.21	0.20	0.27	0.23	...	...	0.06	0.03
HD 177249	0.20	0.07	...	...	0.20	0.06	0.08	0.08	0.08	0.01

**Notes.**  $\sigma_{\text{line}}$  denotes the mean line-to-line scatter.

<sup>a</sup> The *H*-band spectrum of Arcturus is from Hinkle et al. (1995).

<sup>b</sup> The *H*-band spectrum of Arcturus is from the NMSU 1m+APOGEE.

**Table 5**  
Stellar Silicon LTE and NLTE Abundances

Star	$T_{\text{eff}}$	$\log g$	[Fe/H]	$\xi_r$	[Si I <sub>LTE</sub> /Fe](ir)	[Si I <sub>NLTE</sub> /Fe](ir)	$\Delta_{\text{ir}}$	[Si I <sub>LTE</sub> /Fe](opt)	[Si I <sub>NLTE</sub> /Fe](opt)	$\Delta_{\text{opt}}$
Arcturus <sup>a</sup>	4275	1.67	-0.58	1.60	0.43 ± 0.05	0.37 ± 0.04	-0.06	0.35 ± 0.03	0.29 ± 0.02	-0.06
Arcturus <sup>b</sup>	4275	1.67	-0.58	1.60	0.43 ± 0.07	0.37 ± 0.05	-0.06	...	...	...
HD 87	5053	2.71	-0.10	1.35	0.18 ± 0.04	0.12 ± 0.03	-0.06	0.15 ± 0.03	0.12 ± 0.01	-0.03
HD 6582	5390	4.42	-0.81	0.90	0.25 ± 0.02	0.23 ± 0.03	-0.02	0.27 ± 0.02	0.27 ± 0.02	0.00
HD 6920	5845	3.45	-0.06	1.40	0.06 ± 0.08	-0.02 ± 0.02	-0.08	0.05 ± 0.05	0.02 ± 0.03	-0.03
HD 22675	4901	2.76	-0.05	1.30	0.11 ± 0.04	0.05 ± 0.02	-0.06	0.11 ± 0.04	0.07 ± 0.02	-0.04
HD 31501	5320	4.45	-0.40	1.00	0.17 ± 0.04	0.14 ± 0.05	-0.03	0.22 ± 0.02	0.21 ± 0.02	-0.01
HD 58367	4932	1.79	-0.18	2.00	0.18 ± 0.12	0.08 ± 0.06	-0.10	0.16 ± 0.05	0.13 ± 0.02	-0.03
HD 67447	4933	2.17	-0.05	2.12	0.16 ± 0.10	0.07 ± 0.02	-0.09	0.12 ± 0.04	0.08 ± 0.02	-0.04
HD 102870	6070	4.08	0.20	1.20	-0.05 ± 0.03	-0.09 ± 0.01	-0.04	-0.07 ± 0.02	-0.08 ± 0.02	-0.01
HD 103095	5085	4.65	-1.35	0.80	0.32 ± 0.06	0.32 ± 0.07	0.00	0.30 ± 0.04	0.30 ± 0.04	0.00
HD 121370	6020	3.80	0.28	1.40	0.16 ± 0.05	0.11 ± 0.06	-0.05	0.22 ± 0.05	0.19 ± 0.03	-0.03
HD 148816	5830	4.10	-0.73	1.40	0.26 ± 0.05	0.22 ± 0.02	-0.04	0.18 ± 0.03	0.18 ± 0.03	0.00
HD 177249	5273	2.66	0.03	1.65	0.16 ± 0.07	0.07 ± 0.01	-0.09	0.05 ± 0.04	0.03 ± 0.02	-0.02

**Notes.**  $\Delta_{\text{ir}}$  and  $\Delta_{\text{opt}}$  stand for the NLTE effects ( $\Delta = \log \epsilon_{\text{NLTE}} - \log \epsilon_{\text{LTE}}$ ) derived from IR and optical spectra, respectively.

<sup>a</sup> The *H*-band spectrum of Arcturus is from Hinkle et al. (1995).

<sup>b</sup> The *H*-band spectrum of Arcturus is from the NMSU 1m+APOGEE.

(see Table 3). A comparison between the calculated *H*-band line profiles and the observed solar spectrum is shown in Figure 3. In this figure, the NLTE (black solid) lines agree well with the observed spectrum for the strong lines at 15888 and 16680 Å, while the LTE (red dotted) line profiles are weaker. This issue is more obvious for Arcturus, as presented in Figure 4. Figure 5 gives the synthetic profiles at 16680 Å under LTE and NLTE for HD 87. The black solid line denotes the best fit to the observed spectrum in NLTE with a [Si/Fe] of 0.12 dex. The red dotted curve is produced with the same [Si/Fe] in LTE, which is shallower in the line core.

In Table 4 we present the Si abundances derived from the individual *H*-band lines and the mean line-to-line scatter under NLTE and LTE for all sample stars. As indicated in this table,

relative to LTE, NLTE obviously reduces the line-to-line scatter in the derived abundances for some stars. Taking HD 67447 as an example, the mean line-to-line scatter is reduced from 0.12 in LTE to 0.03 dex in NLTE. Table 5 gives the mean abundances along with the standard deviation. As shown in this table, the largest standard deviation in LTE is 0.12 dex, but it decreases to 0.07 dex when the NLTE effects are considered.

According to Table 4, the NLTE effects differ from line to line, and they are larger for strong lines. In our four *H*-band lines, NLTE effects are relatively strong for the Si I lines at 15888 and 16680 Å, while they are weaker for the others. Table 5 also shows the mean NLTE corrections for individual stars, and the NLTE effects range from -0.1 to 0.0 dex.

**Table 6**  
Line Data, Iron Abundances Derived from the Solar Spectrum, and Equivalent Widths of the Solar Lines

$\lambda$	$\chi$	$\log C_6$	$\log gf$	Reference	$\log \varepsilon_{\odot} \text{Fe}$ LTE	$\log \varepsilon_{\odot} \text{Fe}$ NLTE	$\log gf'$	EW
( $\text{\AA}$ )	(eV)				(dex)	(dex)		(m $\text{\AA}$ )
Fe I								
4661.534	4.558	-29.481	-1.27	FUH88	7.57	7.61	-1.16	40.5
4808.149	3.251	-31.464	-2.79	FUH88	7.66	7.70	-2.59	29.5
4885.430	3.882	-30.173	-1.02	KUR14	7.49	7.55	-0.97	91.3
5223.186	3.635	-31.165	-1.78	BRI91	7.05	7.09	-2.19	31.0
5242.497	3.634	-31.248	-0.97	BRI91	7.56	7.52	-0.95	90.3
5379.579	4.154	-31.242	-1.51	BRI91	7.57	7.57	-1.44	63.5
5398.279	4.371	-30.155	-0.67	FUH88	7.55	7.59	-0.58	78.8
5522.449	4.217	-30.457	-1.55	FUH88	7.63	7.68	-1.37	44.9
5546.506	4.434	-30.356	-1.31	FUH88	7.68	7.74	-1.07	52.7
5618.633	4.386	-30.475	-1.28	BRI91	7.49	7.55	-1.23	52.2
5651.469	4.386	-30.264	-2.00	FUH88	7.77	7.78	-1.72	19.5
5679.023	4.186	-30.040	-0.92	FUH88	7.72	7.78	-0.64	65.0
5793.915	4.220	-30.505	-1.70	FUH88	7.58	7.63	-1.57	35.5
5853.148	1.485	-31.586	-5.28	FUH88	7.64	7.67	-5.11	8.1
5855.077	4.608	-30.189	-1.48	BAR94	7.43	7.48	-1.50	23.3
5929.677	4.548	-30.305	-1.41	FUH88	7.71	7.77	-1.14	41.7
6024.058	4.548	-30.358	-0.12	FUH88	7.66	7.70	0.08	127.5
6078.491	4.796	-29.749	-0.32	KUR14	7.47	7.52	-0.30	84.6
6079.009	4.652	-30.237	-1.12	FUH88	7.64	7.70	-0.92	48.8
6151.623	2.176	-31.538	-3.30	FUH88	7.53	7.55	-3.25	51.6
6173.335	2.223	-31.523	-2.88	FUH88	7.56	7.58	-2.80	70.1
6200.321	2.608	-31.279	-2.44	FUH88	7.59	7.59	-2.35	75.2
6240.646	2.223	-31.450	-3.23	BAR91	7.44	7.46	-3.27	48.7
6322.686	2.588	-31.296	-2.43	FUH88	7.60	7.60	-2.33	77.6
6335.331	2.198	-31.546	-2.18	BRI91	7.46	7.46	-2.22	103.3
6481.877	2.279	-31.420	-2.98	FUH88	7.58	7.60	-2.88	65.7
6593.871	2.433	-31.375	-2.42	FUH88	7.62	7.63	-2.29	98.7
6726.666	4.607	-30.256	-1.09	KUR14	7.56	7.63	-0.96	50.2
6839.831	2.559	-31.346	-3.45	FUH88	7.55	7.58	-3.37	30.3
6857.250	4.076	-30.895	-2.15	FUH88	7.56	7.61	-2.04	23.4
mean	...	...	...	...	7.56	7.60	...	...
$\sigma$	...	...	...	...	0.13	0.13	...	...
Fe II								
4508.288	2.856	-31.971	-2.25	RYA99	7.48	7.48	-2.27	77.6
5264.808	3.230	-31.977	-3.12	RYA99	7.53	7.53	-3.09	103.3
5414.073	3.221	-31.976	-3.54	RYA99	7.45	7.45	-3.60	65.7
5991.376	3.153	-31.983	-3.54	BLA80	7.43	7.43	-3.61	98.7
6149.258	3.889	-32.048	-2.72	BLA80	7.49	7.49	-2.73	50.2
6456.383	3.903	-31.979	-2.10	BLA80	7.54	7.54	-2.07	30.3
mean	...	...	...	...	7.49	7.49	...	...
$\sigma$	...	...	...	...	0.04	0.04	...	...

**Note.** References to the  $\log gf$  values are FUH88: Fuhr et al. (1988), KUR14: Kurucz (2014), BRI91: O'Brian et al. (1991), BAR94: Bard & Kock (1994), BAR91: Bard et al. (1991), RYA99: Ryabchikova et al. (1999) and BLA80: Blackwell et al. (1980). The  $\log C_6$  values were calculated according to Anstee & O'Mara (1991, 1995) and Barklem et al. (2000).  $\sigma$  refers to the statistical error. The  $\log gf'$  denotes that the  $gf$ -values were derived from the NLTE solar fits.

To explore the dependency of the NLTE corrections on stellar parameters, we plot the difference of the  $[\text{Si}/\text{Fe}]$  derived under NLTE and LTE assumptions for the strong silicon lines (15888 and 16680  $\text{\AA}$ ) as functions of metallicity, effective temperature, and surface gravity in Figure 6. It can be seen that the NLTE corrections of the  $H$ -band lines are negative, which means that the Si abundances would be overestimated under LTE. The NLTE effects, on the other hand, are very sensitive to the surface gravity, the absolute corrections increase with the decreasing surface gravity, and the largest correction reaches  $\sim 0.2$  dex for HD 58367. Since surface gravity effects dominate, we do not see clear trends in

the NLTE corrections with metallicity and effective temperature in these figures. In order to investigate the NLTE corrections for APOGEE data in extreme cases, we calculated the NLTE and LTE line profiles of the Si I line at 15888  $\text{\AA}$  with parameters  $T_{\text{eff}} = 5000$  K,  $[\text{Fe}/\text{H}] = 0.0$  dex,  $\log g = 0.5$ ,  $\xi_t = 2.0$  km s $^{-1}$ . As shown in Figure 7, when  $[\text{Si}/\text{Fe}]$  under NLTE and LTE shares the same value, namely  $[\text{Si}/\text{Fe}] = 0.0$  dex, the two profiles are different. By increasing  $[\text{Si}/\text{Fe}]$ , the line cores of LTE spectra tend to be deeper, and until  $[\text{Si}/\text{Fe}]$  reaches 0.39 dex, the LTE profile best fits the synthetic NLTE profile. That is to say that in this extreme case, the NLTE correction can reach  $\sim -0.4$  dex.

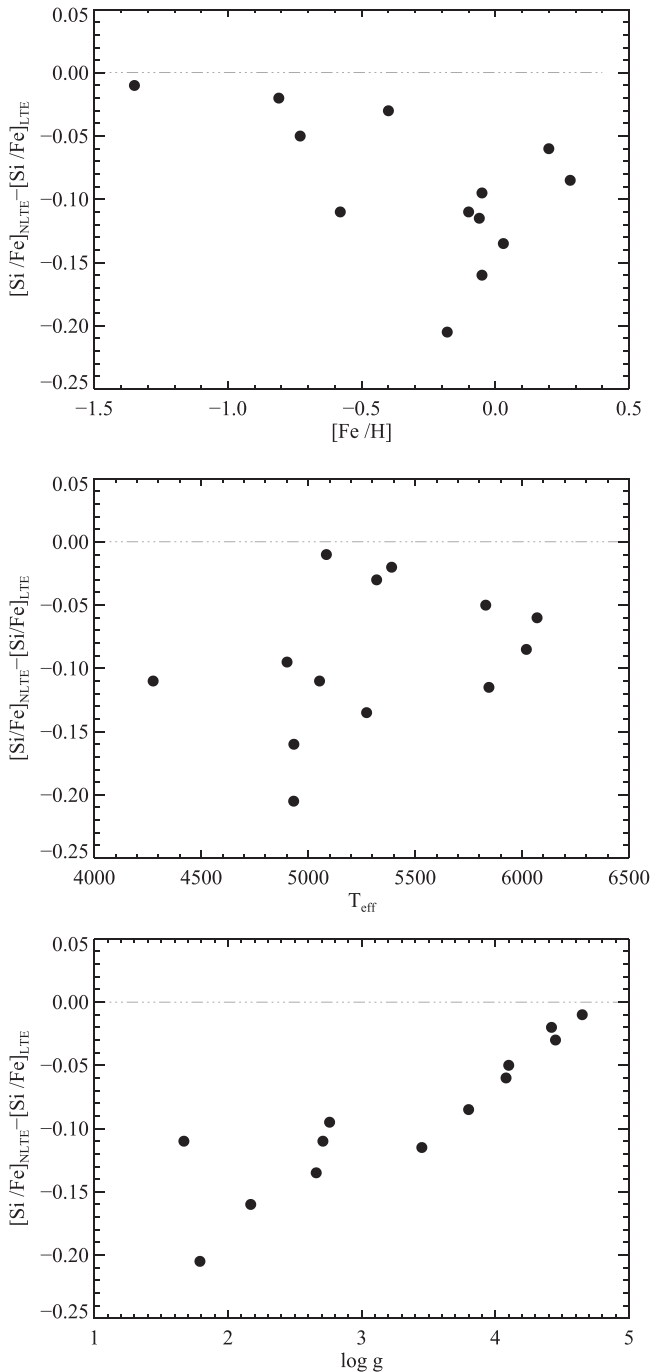


**Figure 6.** The mean NLTE corrections for the two strong Si I lines at 15888 and 16680 Å as functions of  $[\text{Fe}/\text{H}]$ ,  $T_{\text{eff}}$ , and  $\log g$ , respectively (from top to bottom).

To test whether consistent abundances are obtained from spectra acquired with different telescopes or instruments, we derived the Si abundance of Arcturus with the spectrum from Hinkle et al. (1995) ( $R \sim 100,000$ ) and the 1m+APOGEE spectrum ( $R \sim 22,500$ ). Figure 8 shows the best-fitting NLTE profiles for the two observed spectra. The left panel shows the Arcturus spectrum from Hinkle et al. (1995), while the right panel is for the 1m+APOGEE spectrum. Their results for individual lines are listed in Table 4, and the mean values for each line are collected in Table 5. The difference of abundances

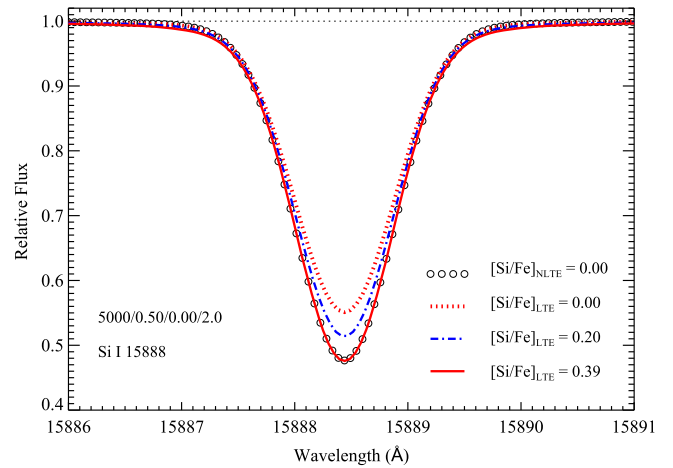


**Figure 7.** The LTE and NLTE synthetic spectra of Si I 15888 Å line with different  $[\text{Si}/\text{Fe}]$  values and the same parameters of  $T_{\text{eff}} = 5000$  K,  $\log g = 0.5$ , and  $[\text{Fe}/\text{H}] = 0.0$ ,  $\xi_T = 2.0$ .  $[\text{Si}/\text{Fe}] = 0.00$ , 0.20, and 0.39 dex for the LTE line profiles, while  $[\text{Si}/\text{Fe}] = 0.00$  for the NLTE calculation.

derived from individual lines between the two spectra is negligible,  $\leq 0.02$  dex. A consistent Si abundance is acquired for the same object from different telescopes or instruments.

### 5.2.2. Departures from LTE for Si I Optical Lines

We investigated the eight Si I optical lines described in Section 5.1.2 for our sample stars. The mean Si abundances under LTE and NLTE are presented in Table 5. As shown in this table, the standard deviations are very small, lower than 0.05 dex for both LTE and NLTE abundances; the net NLTE correction for a given star is minor, with an absolute value lower than 0.06 dex. Although the mean NLTE corrections are small, the NLTE effects are necessary for the strongest investigated Si I lines, e.g., the largest NLTE correction for the line at 6155 Å reaches  $\sim 0.1$  dex in our sample according to Table 7. The corrections could be greater in extreme cases.

### 5.2.3. Comparison with the Optical Results and Discussions

For our sample stars, the differences between the mean Si abundances derived from IR and from optical spectra are shown against the metallicity in Figure 9. In this figure, open circles denote the differences in LTE, while filled circles indicate the NLTE results. The differences between LTE and NLTE are evidently small (lower than 0.1 dex), and the derived Si abundances from the  $H$ -band spectral lines agree better with those from optical lines in NLTE than in LTE. Since the NLTE effects are larger for strong lines, it is interesting to see whether the Si abundances derived when only  $H$ -band strong lines at 15888 and 16680 Å are available are still consistent with those from optical lines. The differences between the abundances derived from the two strong  $H$ -band lines and from optical lines are depicted in Figure 10. Similar to Figure 9, the NLTE Si abundances from the strong  $H$ -band lines are consistent with those from optical lines, while the differences become as large as 0.2 dex in LTE.

## 6. CONCLUSIONS

The main purpose of this work is to test the validity of the Si atomic model for the  $H$ -band line formation and to investigate

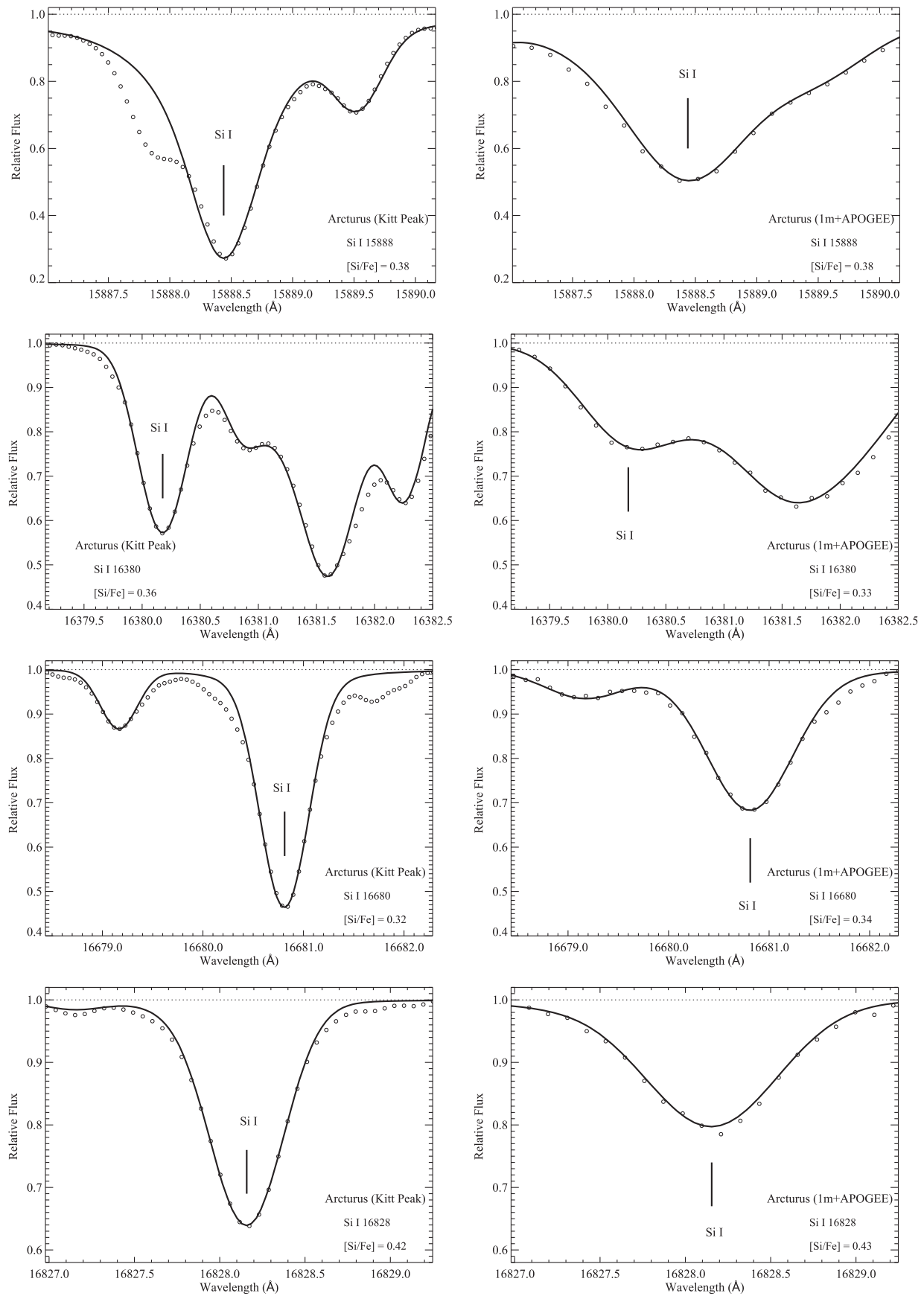


**Figure 8.** The best-fitting NLTE profiles (solid lines) of the four investigated Si I lines in the Kitt Peak (Hinkle et al. 1995) and 1m+APOGEE observed spectra of Arcturus (open circles). The left panel shows the spectrum of Arcturus from Hinkle et al. (1995), while the right panel is for the 1m+APOGEE spectrum.

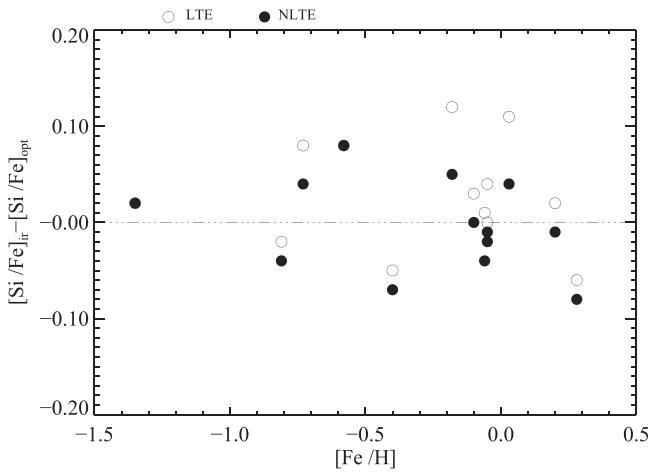


**Figure 9.** The difference between the mean Si abundances derived from IR and optical lines under LTE (open circles) and NLTE (filled circles) assumptions.

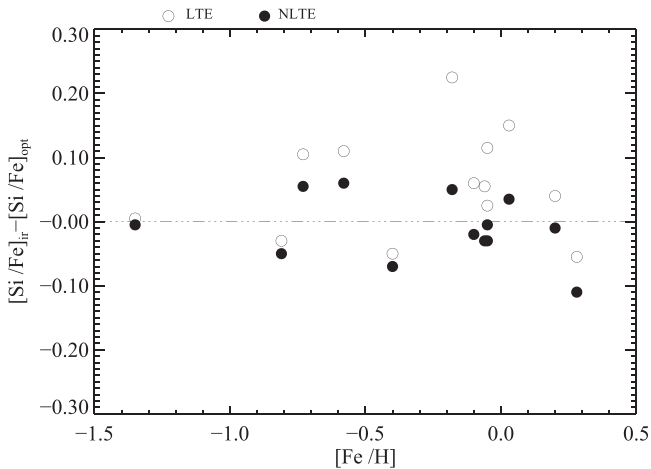


**Figure 10.** The difference between the Si abundances derived from the two strong Si I lines at 15888 and 16680 Å and the optical lines under LTE (open circles) and NLTE (filled circles).

the NLTE effects on Si spectral lines based on high S/N IR  $H$ -band spectra. A sample of 13 FGK dwarfs and giants was selected, and the Si abundances were derived from both  $H$ -band and optical lines under LTE and NLTE.

After careful analyses, we list our conclusions below.

1. With a NLTE analysis, the absolute differences between the mean Si abundances from the  $H$ -band and from optical lines are lower than 0.1 dex for the sample stars, which suggests that our Si atomic model can be applied to investigate the formation of the  $H$ -band Si I lines.
2. The NLTE effects differ from line to line. The strong Si I lines at 15888 and 16680 Å need large NLTE corrections, while the other two lines show weaker NLTE effects. Thus, it is not surprising that the NLTE silicon abundance shows a smaller line-to-line scatter than the LTE abundance for some stars in this analysis. The NLTE corrections reach  $\sim -0.2$  dex for the strongest Si I line in our sample. It can be up to  $\sim -0.4$  dex for the extreme cases of APOGEE targets ( $\log g \sim 0.5$ ). This shows that it should be

considered in the abundance analysis, especially for the cases where only strong lines are available.

3. The NLTE effects are sensitive to the surface gravity, and increase with decreasing surface gravities.
4. The NLTE corrections for the investigated  $H$ -band lines are negative, which means that the Si abundances derived with a LTE assumption are overestimated.

To the best of our knowledge, this work is the first NLTE investigation of the  $H$ -band Si spectral lines. The NLTE corrections of strong lines range from  $-0.2$  to  $-0.1$  dex for giant stars in our sample. In extreme cases of APOGEE targets, the correction could be up to  $-0.4$  dex. Thus they may have a significant impact on the Si abundances derived from APOGEE observations. Motivated by these results, the APOGEE team is planning to pursue more extended NLTE calculations in the coming years.

This research is supported by National Key Basic Research Program of China 2014CB845700, and by the National Natural Science Foundation of China under grant Nos. 11321064, 11233004, 11390371, 11473033, 11428308, U1331122. C.A.P. is thankful to the Spanish MINECO for support through grant AYA2014-56359-P.

We acknowledge the support of the staff of the Xinglong 2.16 m telescope. This work was partially supported by the Open Project Program of the Key Laboratory of Optical Astronomy, National Astronomical Observatories, Chinese Academy of Sciences. We thank Yoichi Takeda, Bun'ei Sato, and Yujian Liu for providing us the optical data. The authors thank the anonymous referee for comments that helped to improve the manuscript.

This research uses services or data provided by the NOAO Science Archive. NOAO is operated by the Association of Universities for Research in Astronomy (AURA), Inc. under a cooperative agreement with the National Science Foundation.

This work has made use of the VALD database, operated at Uppsala University, the Institute of Astronomy RAS in Moscow, and the University of Vienna.

Funding for SDSS-III has been provided by the Alfred P. Sloan Foundation, the Participating Institutions, the National Science Foundation, and the U.S. Department of Energy Office of Science. The SDSS-III website is <http://www.sdss3.org/>.

SDSS-III is managed by the Astrophysical Research Consortium for the Participating Institutions of the SDSS-III Collaboration including the University of Arizona, the Brazilian Participation Group, Brookhaven National Laboratory, Carnegie Mellon University, University of Florida, the French Participation Group, the German Participation Group, Harvard University, the Instituto de Astrofísica de Canarias, the Michigan State/Notre Dame/JINA Participation Group, Johns Hopkins University, Lawrence Berkeley National Laboratory, Max Planck Institute for Astrophysics, Max Planck Institute for Extraterrestrial Physics, New Mexico State University, New York University, Ohio State University, Pennsylvania State University, University of Portsmouth, Princeton University, the Spanish Participation Group, University of Tokyo, University of Utah, Vanderbilt University, University of Virginia, University of Washington, and Yale University.

## APPENDIX

**Table 7**  
Silicon Relative to Iron Abundances Based on Optical Si I Lines under LTE and NLTE Analyses

Star	5701 (Å)		5772 (Å)		6142 (Å)		6145 (Å)		6155 (Å)		6237 (Å)		6243 (Å)		6244 (Å)	
	LTE	NLTE														
Arcturus	0.32	0.27	...	...	0.31	0.28	...	...	0.38	0.28	0.36	0.30	0.36	0.32	...	...
HD 87	0.15	0.12	0.19	0.13	0.12	0.11	0.14	0.13	0.13	0.13	...	...	...	...	...	...
HD 6582	0.27	0.27	0.27	0.26	...	...	0.27	0.27	0.26	0.25	0.23	0.23	0.31	0.31	0.27	0.27
HD 6920	...	...	0.06	0.03	...	...	0.00	-0.01	0.10	0.05	...	...	...	...	...	...
HD 22675	0.11	0.08	0.14	0.07	0.07	0.05	0.08	0.06	0.17	0.10	...	...	...	...	...	...
HD 31501	0.21	0.20	...	...	0.18	0.18	0.23	0.22	0.22	0.20	...	...	0.25	0.24	0.22	0.21
HD 58367	0.15	0.11	...	...	0.11	0.11	0.13	0.13	0.23	0.15	...	...	...	...	...	...
HD 67447	0.11	0.07	0.15	0.08	0.06	0.05	0.10	0.09	0.17	0.08	0.15	0.10	0.08	0.06	0.13	0.09
HD 102870	-0.09	-0.10	-0.05	-0.07	-0.08	-0.08	-0.06	-0.06	-0.03	-0.05	-0.09	-0.10	-0.07	-0.07	-0.09	-0.09
HD 103095	0.36	0.35	...	...	...	...	...	...	0.25	0.25	0.30	0.30	0.32	0.32	0.28	0.28
HD 121370	...	...	0.21	0.18	0.17	0.17	0.17	0.17	0.29	0.23	0.24	0.21	...	...	...	...
HD 148816	...	...	0.18	0.17	0.14	0.14	0.23	0.23	0.17	0.16	0.17	0.17	0.18	0.18	0.19	0.19
HD 177249	0.04	0.02	...	...	0.05	0.05	0.02	0.02	0.13	0.07	...	...	...	...	...	...

**Table 8**  
Equivalent Widths of Neutral Iron Lines for Sample Stars

$\lambda$ (Å)	Arcturus	HD 87	HD 6582	HD 6920	HD 22675	HD 31501	HD 58367	HD 67447	HD 102870	HD 103095	HD 121370	HD 148816	HD 177249
4661.534	...	...	18.0	39.8	...	...	...	89.5	40.4	8.0	48.7	10.4	...
4808.149	...	...	11.5	25.6	...	...	...	72.4	28.8	8.4	37.1	7.1	...
4885.430	...	...	55.7	75.3	...	...	...	126.2	77.8	38.1	87.9	37.7	...
5223.186	64.3	52.0	14.7	32.5	61.5	...	...	67.8	30.7	8.7	37.3	7.2	...
5242.497	117.5	115.9	63.6	92.2	120.9	...	146.5	146.4	92.0	54.9	108.0	54.8	121.6
5379.579	90.9	87.5	38.1	59.5	93.8	...	111.4	114.7	63.7	22.4	76.1	27.7	93.4
5398.279	91.1	94.7	48.3	71.0	104.2	...	116.8	124.5	78.9	33.2	88.7	38.5	102.9
5522.449	61.0	66.2	20.1	41.5	71.1	...	78.8	84.3	44.1	10.6	57.0	14.3	69.8
5546.506	72.2	75.1	26.0	51.0	81.7	...	91.6	100.4	53.4	14.1	68.8	17.7	80.4
5618.633	71.0	69.4	27.4	50.3	76.0	42.3	88.9	93.6	53.2	12.3	65.3	18.4	77.6
5651.469	32.2	33.5	6.6	18.8	39.7	14.6	45.7	45.1	19.2	...	27.3	...	35.8
5679.023	70.0	76.4	32.8	61.2	81.9	53.7	87.9	97.2	60.8	17.1	72.0	24.0	81.5
5793.915	53.6	58.6	12.9	29.8	62.1	28.1	70.0	84.6	34.4	6.1	45.9	9.3	72.0
5853.148	...	...	...	...	44.2	12.0	45.1	51.5	6.0	...	10.5	...	27.4
5855.077	34.2	39.9	7.8	22.0	43.9	17.5	...	49.5	23.0	...	31.2	5.3	39.2
5929.677	54.7	63.3	16.3	...	67.6	37.7	73.9	78.0	40.4	17.0	50.9	17.0	63.4
6024.058	116.8	125.7	87.0	107.5	132.6	120.1	...	156.0	114.0	70.3	124.7	66.7	135.0
6078.491	81.2	93.8	47.5	76.6	99.0	81.2	...	117.0	82.5	29.5	92.8	35.2	99.2
6079.009	58.3	62.9	19.3	40.7	69.7	41.6	80.0	85.4	48.9	9.2	54.2	13.7	70.1
6151.623	114.6	88.1	31.3	47.5	97.9	51.4	117.4	122.1	45.4	21.4	54.7	17.4	91.5
6173.335	133.0	109.5	48.3	70.3	119.9	52.3	146.8	148.9	66.0	40.0	78.0	33.7	115.1
6200.321	132.7	111.0	52.2	73.0	121.7	74.2	140.3	148.0	78.8	41.4	87.1	34.5	116.4
6240.646	114.7	...	29.8	43.7	...	52.3	...	127.4	43.2	19.8	55.2	16.5	...
6322.686	140.7	...	53.8	76.8	...	76.7	...	150.6	73.0	44.3	91.0	40.6	...
6335.331	132.6	...	85.1	103.5	...	109.1	...	196.0	98.4	79.2	115.3	66.2	...
6481.877	...	...	...	63.9	...	72.4	...	142.9	62.4	34.1	76.6	27.5	...
6593.871	...	...	68.8	89.1	...	90.6	...	177.7	93.9	61.3	101.1	55.4	...
6726.666	...	...	19.8	50.0	...	42.1	...	86.6	49.6	9.8	62.8	15.3	...
6839.831	...	...	15.3	...	...	32.2	...	94.5	28.9	8.2	43.5	7.2	...
6857.250	...	...	...	...	...	18.8	...	55.3	...	...	...	5.9	...

**Note.** Strongly blended lines and lines with poor S/N were rejected when we determined the stellar parameters for a given star.

## REFERENCES

- Ahn, C. P., Alexandroff, R., Allende Prieto, C., et al. 2014, *ApJS*, 211, 17
- Alam, S., Albareti, F. D., Allende Prieto, C., et al. 2015, *ApJS*, 219, 12
- Alonso, A., Arribas, S., & Martínez-Roger, C. 1996, *A&A*, 313, 873
- Alonso, A., Arribas, S., & Martínez-Roger, C. 1999, *A&AS*, 140, 261
- Alonso, A., Arribas, S., & Martínez-Roger, C. 2001, *A&A*, 376, 1039
- Amarsi, A. M., & Asplund, M. 2016, arXiv:1609.07283
- Anstee, S. D., & O'Mara, B. J. 1991, *MNRAS*, 253, 549
- Anstee, S. D., & O'Mara, B. J. 1995, *MNRAS*, 276, 859
- Bard, A., Kock, A., & Kock, M. 1991, *A&A*, 248, 315
- Bard, A., & Kock, M. 1994, *A&A*, 282, 1014
- Barklem, P. S., & O'Mara, B. J. 1997, *MNRAS*, 290, 102
- Barklem, P. S., O'Mara, B. J., & Ross, J. E. 1998, *MNRAS*, 296, 1057
- Barklem, P. S., Piskunov, N., & O'Mara, B. J. 2000, *A&AS*, 142, 467
- Belyaev, A. K., Yakovleva, S. A., & Barklem, P. S. 2014, *A&A*, 572, A103
- Bensby, T., Feltzing, S., Lundström, I., et al. 2005, *A&A*, 433, 185
- Bensby, T., Feltzing, S., & Oey, M. S. 2014, *A&A*, 562, A71
- Bergemann, M., Kudritzki, R. P., Würfl, M., et al. 2013, *ApJ*, 764, 115
- Blackwell, D. E., Shallis, M. J., & Simmons, G. J. 1980, *A&A*, 81, 340
- Butler, K., & Giddings, J. 1985, Newsletter on the Analysis of Astronomical Spectra (Univ. London)
- Eisenstein, D. J., Weinberg, D. H., Agol, E., et al. 2011, *AJ*, 142, 72
- Feuillet, D. K., Bovy, J., Holtzman, J., et al. 2016, *ApJ*, 817, 40
- Fuhr, J. R., Martin, G. A., & Wiese, W. L. 1988, *JPCRD*, 17, 4
- Fuhrmann, K. 1998, *A&A*, 338, 161
- García Pérez, A. E., Allende Prieto, C., Holtzman, J. A., et al. 2016, *AJ*, 151, 144
- Garz, T. 1973, *A&A*, 26, 471
- Goswami, A., & Prantzos, N. 2000, *A&A*, 359, 191
- Grevesse, N., Asplund, M., & Sauval, A. J. 2007, *SSRv*, 130, 105
- Gustafsson, B., Edvardsson, B., Eriksson, K., et al. 2008, *A&A*, 486, 951
- Hall, D. N. B., Ridgway, S. T., Bell, E. A., et al. 1979, *Proc. SPIE*, 172, 121
- Hawkins, K., Masseron, T., Jofre, P., et al. 2016, arXiv:1604.08800
- Henyey, L., Vardya, M. S., & Bodenheimer, P. 1965, *ApJ*, 142, 841
- Hinkle, K., & Wallace, L. 2005, in *ASP Conf. Ser. 336, Cosmic Abundances as Records of Stellar Evolution and Nucleosynthesis*, ed. T. G. Barnes, III & F. N. Bash (San Francisco, CA: ASP), 321
- Hinkle, K., Wallace, L., & Livingston, W. 1995, *PASP*, 107, 1042
- Hinkle, K., Wallace, L., Valenti, J., et al. 2000, *Visible and Near Infrared Atlas of the Arcturus Spectrum 3727-9300 Å* (San Francisco, CA: ASP)
- Holtzman, J. A., Shetrone, M., Johnson, J. A., et al. 2015, *AJ*, 150, 148
- Holweger, H. 1973, *A&A*, 26, 275
- Izumiura, H. 2003, *AstHe*, 96, 291
- Johnson, T. V., Mousis, O., Lunine, J. I., & Madhusudhan, N. , 2011, *LPICo*, 1639, 9011
- Kamp, L. W. 1973, *ApJ*, 180, 447
- Kamp, L. W. 1978, *ApJ*, 36, 143
- Kamp, L. W. 1982, *ApJ*, 48, 415
- Kelleher, D. E., & Podobedova, L. I. 2008, *JPCRD*, 37, 1285
- Kobayashi, C., Karakas, A. I., & Umeda, H. 2011, *MNRAS*, 414, 3231
- Kurucz, R. L. 2007, Robert L. Kurucz Online Database of Observed and Predicted Atomic Transitions, <http://kurucz.harvard.edu>
- Kurucz, R. L. 2014, Robert L. Kurucz Online Database of Observed and Predicted Atomic Transitions, <http://kurucz.harvard.edu>
- Kurucz, R. L., Furenlid, I., Brault, J., et al. 1984, *Solar Flux Atlas from 296 to 1300 nm* (Sunspot, NM: National Solar Observatory)
- Lee, Y. S., Beers, T. C., An, D., et al. 2011, *ApJ*, 738, 187
- Majewski, S. R., Schiavon, R. P., Allende Prieto, C., et al. 2015, arXiv:1509.05420
- Mashonkina, L., Gehren, T., Shi, J. R., et al. 2011, *A&A*, 528, A87
- Mashonkina, L., Korn, A. J., & Przybilla, N. 2007, *A&A*, 461, 261
- Meléndez, J., & Barbuy, B. 1999, *ApJS*, 124, 527
- Mészáros, S., Holtzman, J., García Pérez, A. E., et al. 2013, *AJ*, 146, 133
- Nahar, S. N., & Pradhan, A. K. 1993, *JPhB*, 26, 1109
- Nidever, D. L., Holtzman, J. A., Allende Prieto, C., et al. 2015, *AJ*, 150, 173
- Nissen, P. E., & Schuster, W. J. 2010, *A&A*, 511, L10
- O'Brian, T. R., Wickliffe, M. E., Lawler, J. E., et al. 1991, *JOSAB*, 8, 1185
- Pfeiffer, M. J., Frank, C., Baumüller, D., et al. 1998, *A&AS*, 130, 381
- Ramírez, I., & Allende Prieto, C. 2011, *ApJ*, 743, 135
- Reddy, B. E., Lambert, D. L., & Allende Prieto, C. 2006, *MNRAS*, 367, 1329
- Reddy, B. E., Tomkin, J., Lambert, D. L., et al. 2003, *MNRAS*, 340, 304
- Reetz, J. K. 1991, Diploma thesis, Universität München
- Romano, D., Karakas, A. I., Tosi, M., et al. 2010, *A&A*, 522, A32
- Ryabchikova, T. A., Piskunov, N. E., Stempels, H. C., et al. 1999, *PhST*, 83, 162
- Rybicki, G. B., & Hummer, D. G. 1991, *A&A*, 245, 171
- Rybicki, G. B., & Hummer, D. G. 1992, *A&A*, 262, 209
- Samland, M. 1998, *ApJ*, 496, 155
- Sheminova, V. A. 2015, *KPCB*, 31, 172
- Shi, J. R., Gehren, T., Butler, K., et al. 2008, *A&A*, 486, 303
- Shi, J. R., Gehren, T., Mashonkina, L., et al. 2009, *A&A*, 503, 533
- Shi, J. R., Gehren, T., & Zhao, G. 2011, *A&A*, 534, A103
- Shi, J. R., Takada-Hidai, M., Takeda, Y., et al. 2012, *ApJ*, 755, 36
- Takeda, Y., Sato, B., & Murata, D. 2008, *PASJ*, 60, 781
- Tsujimoto, T., Nomoto, K., Yoshii, Y., et al. 1995, *MNRAS*, 277, 945
- Wang, X. M., Shi, J. R., & Zhao, G. 2009, *MNRAS*, 399, 1264
- Wedemeyer, S. 2001, *A&A*, 2001, 998
- Wilson, J. C., Hearty, F., Skrutskie, M. F., et al. 2010, *Proc. SPIE*, 7735, 77351C
- Woosley, S. E., & Weaver, T. A. 1995, *ApJS*, 101, 181
- Zambardi, T., Poitrasson, F., Corgne, A., et al. 2013, *GeCoA*, 121, 67
- Zhang, L., Karlsson, T., Christlieb, N., et al. 2011, *A&A*, 528, A92
- Zhao, G., & Li, H. B. 2001, *ChJAA*, 1, 555